energies

Article

Theoretical and Experimental Studies of a PDMS Pneumatic Microactuator for Microfluidic Systems

Xuling Liu [1], Huafeng Song [2], Wensi Zuo [1], Guoyong Ye [1], Shaobo Jin [1], Liangwen Wang [1] and Songjing Li [3,*]

1 School of Mechanical and Electronic Engineering, Zhengzhou University of Light Industry, Zhengzhou 450002, China
2 Henan Xixi Highway Construction Co., Ltd., Nanyang 474450, China
3 Department of Fluid Control and Automation, Harbin Institute of Technology, Harbin 150001, China
* Correspondence: lisongjing@hit.edu.cn

Abstract: The compact, simple, and fast-reaction pneumatic microactuator is significant for the integration and high efficiency of pneumatic systems. In this work, the structure, working principle, and multiphysical model of an on-chip pneumatic microactuator are presented. The on-chip pneumatic microactuator is mainly composed of two parts: a polydimethylsiloxane (PDMS) thin membrane and an actuated chamber. The air pressure in the actuated chamber drives the thin elastic membrane to deformation. Dynamic response mathematical models of the actuated chamber for charging and exhaust with variable volume are established, and the deformation characteristics of the polydimethylsiloxane (PDMS) actuated membrane, the capacity of the actuated chamber, and the valve opening of the on-off membrane microvalve are simulated and analyzed to explore the response characteristics of the proposed pneumatic microactuator. Samples valving analysis of the on-chip membrane microvalve and mixing performance of the micromixer integrated with the pneumatic microactuator are tested to evaluate the driving capability of the pneumatic microactuator, and the results show that the response performance of the actuated time fully satisfies the needs of a pneumatic microfluidic chip for most applications.

Keywords: pneumatic microactuator; multiphysical field; mathematical model; response time; dynamic characteristics

check for updates

Citation: Liu, X.; Song, H.; Zuo, W.; Ye, G.; Jin, S.; Wang, L.; Li, S. Theoretical and Experimental Studies of a PDMS Pneumatic Microactuator for Microfluidic Systems. *Energies* **2022**, *15*, 8731. https://doi.org/10.3390/en15228731

Academic Editors: Marco Marengo and Adrian Ilinca

Received: 5 September 2022
Accepted: 10 November 2022
Published: 20 November 2022

1. Introduction

The great potential of microfluidic chips has developed into a new research field of biology detection, chemistry analysis, drug screening, fluid, electronics, materials, machinery, and other disciplines [1–4]. Due to the micron-scale structure, fluids display and produce special properties in microfluidic chips that are different from those at the macroscopic scale, and unique analytically generated properties have been developed [5–7]. The leap from operation unit composition to super-scale integration has been realized because the control system and pressure generation of the pneumatic microfluidic chip are usually off-chip. This enabled the development of the digital microfluidic chip, which has the advantages of small size, small reagent usage, fast reaction, easy to carry, parallel processing, and easy to realize automation, and has excellent development potential and broad application prospects [8,9].

The pneumatic microactuator is an important component of the membrane microvalve, micropump, micromixer, and other essential features of a pneumatic microfluidic chip [10–12]. Quake et al. studied a high-density microfluidic chip containing thousands of pneumatic microvalves and micropumps for high-throughput, parallelized screening of fluorescence-based single-cell assays. These pneumatic microvalves, also called Quake valves, are driven by pneumatic microactuators [13]. A microrotary mixer formed of three Quake microvalves is applied and used in multiplexing and multistep biochemical processing by Quake's research group [14]. A pneumatic microactuator and a micromixing chamber are integrated to perform a reaction of paramagnetic microbeads, and fluorescent microbeads, and the bioconjugation efficiency is experimentally studied [15]. A polydimethylsiloxane (PDMS) micromixer with an integrated pneumatic microactuator is applied for the preparation and improvement of CdS quantum dots rapid synthesis [16]. Previous studies about pneumatic actuators have focused on encapsulation and specific applications, but studies on its dynamic performance are still not perfect.

The PDMS material employed in microchips has become popular and promising in applications due to its excellent properties. The application of PDMS microchips in biological experiments can form enough stable temperature gradients, which is convenient for the realization of the reaction [17]. In addition, because of its penetrability to ultraviolet and visible light, it can be used with various optical detectors [18]. More importantly, in cell experiments, PDMS has an irreplaceable position compared with other polymer materials due to its nontoxic characteristics and air permeability [19,20]. Significantly, the excellent flexibility [21] enables us to apply it as the deformation part of the pneumatic microactuator, which is critical for the pneumatic microactuator. The PDMS thin membrane employed in the pneumatic actuation is the only moving part. Its structure parameters and dynamic performance are essential for the pneumatic microactuator. To investigate the performance of the PDMS thin membrane, some scholars are dedicated to the study of the size changes and deformation properties of the actuated membrane [22,23]. In summary, various methods are utilized to study the PDMS thin membrane for different design requirements. Nevertheless, the dynamic performance of the PDMS thin membrane, as the actuated component of the pneumatic microactuator, needs further study to evaluate the response characteristics.

Many researchers focus on the impact of the actuated membrane material, actuated chamber dimension, and the deformation of PDMS thin membranes [24,25]. However, the effects on the characteristics of the pneumatic microactuator, such as dynamic response properties and transient air pressure change in the actuated chamber, have not yet been sufficiently studied. In addition, studies on a change of air pressure during the driving process, the response characteristic, and its related factors to the pneumatic microactuator are far from enough and require further investigation. Furthermore, the study of pneumatic microdrive overall performance, such as response and inflatable instant actuated chamber pressure change, is still not perfect.

The purpose of this research is to study the deformation performance of the PDMS thin membrane, response times, and its influencing parameters of the pneumatic microactuator, and this is of great importance [26–28] to improve the overall efficiency for pneumatic microfluidic chips. Mathematical models describing the critical characteristics of the pneumatic microactuator, including the membrane deformation, volume variation, response time, and valve opening of the on-chip microvalve, are derived. In particular, the response performance of the pneumatic microactuator and its influence factors are developed by theory, simulation, and experimental methods in this work. The valving and mixing performance actuated by the proposed pneumatic microactuator is experimented and analyzed to evaluate the driving performance of the pneumatic microactuator. The results show that the undertaking can fully satisfy the needs of a pneumatic microfluidic chip for most applications. The derived mathematical models and experimental methodology can be used to predict the overall response time of a pneumatic microfluidic chip, and provide a theoretical basis for the design of pneumatic device size parameters for reducing the actuated pressure and improving the efficiency of microsystems.

2. System Description

The pneumatic microactuator is the core component of the basic components of the pneumatic microfluidic chip, such as the membrane valve, micropump, and micromixer. The pneumatic microactuator comprises the actuated chamber connected with the air channel and the PDMS thin membrane above the actuated chamber, as shown in Figure 1a.

A three-way microvalve situated in the air channel is used to control the connection between the actuated chamber and the compressed air source and to precisely regulate the flow rate of air entering and exiting the actuated chamber. The air enters the actuated chamber, increases the air pressure, and drives the PDMS thin membrane to deformation. All parts except the actuated area are sealed with a layer of PDMS to prevent deformation of the remaining pneumatic microchannel.

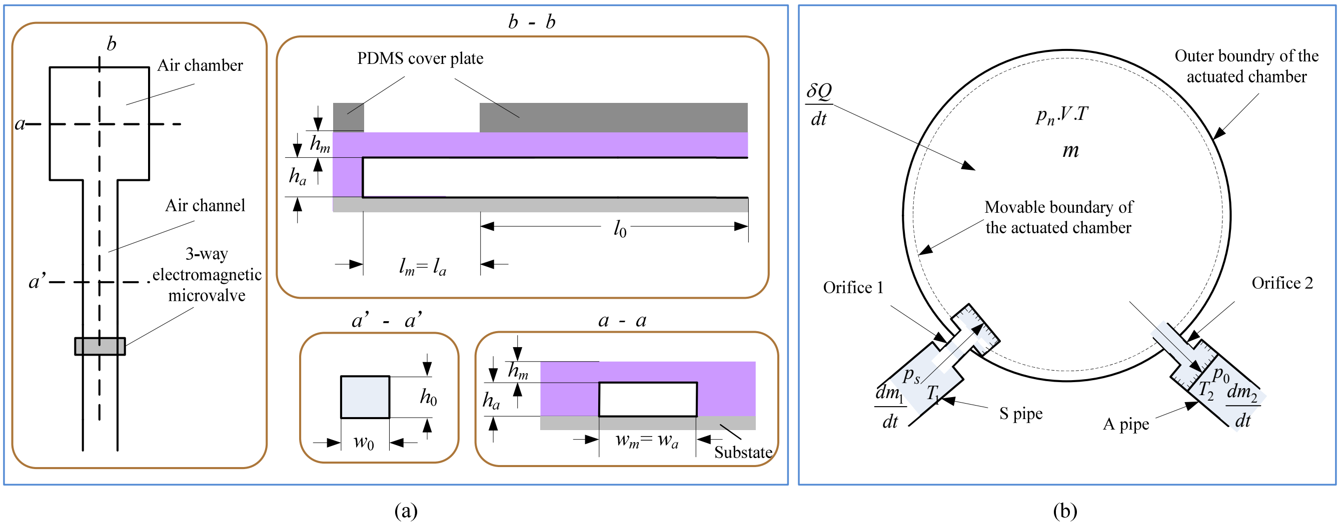

Figure 1. Schematic layout and model of the pneumatic microactuator: (**a**) schematic layout of the pneumatic microactuator; (**b**) model of the actuated chamber with variable volume.

The driving chamber of the pneumatic microactuator can be regarded as an elastic air capacity, whose volume varies with the pressure in the driving chamber. The inflation and exhaust models of the actuated chamber with variable volume are illustrated in Figure 1b. Port S and port A are connected to the air supply and the atmosphere through three-way microvalves, respectively. The constant pressure supply p_s is connected to the S port and inflates the actuated chamber with variable volume. The valve ports of Electromagnetic Microvalve 1 and Electromagnetic Microvalve 2 are inlet and exhaust constraint orifices, respectively. The designed parameter names and the values of the pneumatic microactuator are presented in Table 1.

Table 1. Parameters of the pneumatic microactuator designed for simulation and experimental design.

Parameter	Value (μm)		
	Design Scheme 1	***Design Scheme 2***	***Design Scheme 3***
l_a	500	500	500
l_m	500	500	500
w_a	200	300	500
w_m	200	300	500
h_a	100	100	100
h_0	100	100	100
h_m	40	40	40
l_0	3000	3000	3000
w_0	100	100	100

3. Model of the PDMS Pneumatic Microactuator

In this section, equations are presented to calculate the deflection of the PDMS thin membrane, the variational volume, and the response time of the pneumatic microactuator. The basic equations of the dynamic inflatable process of the pneumatic microactuator include the mathematical model of elastic gas volume change, which is determined by the deformation of the PDMS thin membrane, and the inflatable mathematical model of the pneumatic microactuator. It should be noted that the air permeability of the PDMS membrane is related to its thickness. The N_2 permeability of the PDMS membrane with a thickness of 100 µm is 9.796 * 104 cm^3/24 h·0.1 MPa by experiments. Detailed information about the air permeability of the PDMS thin membrane can be found in the literature [20]. However, because of the negligible air permeability and continuous air supply of the system, the surface air permeability of the PDMS thin membrane is not considered in the subsequent mathematical model and simulation, and it has almost no effect on the subsequent experiments.

3.1. Deformation of the PDMS Thin Membrane

PDMS thin membranes can be virtually regarded as high-elastic nonlinear polymers. According to the large deformation theory of the thin membrane and the plane strain theory of the thin rectangular membrane [29,30], the strain along the Y-direction will not change due to the force on the thin membrane, as shown in Figure 2a,b. Thus, the deformation of the thin rectangular membrane is simplified to a two-dimensional problem, namely, a plane strain problem.

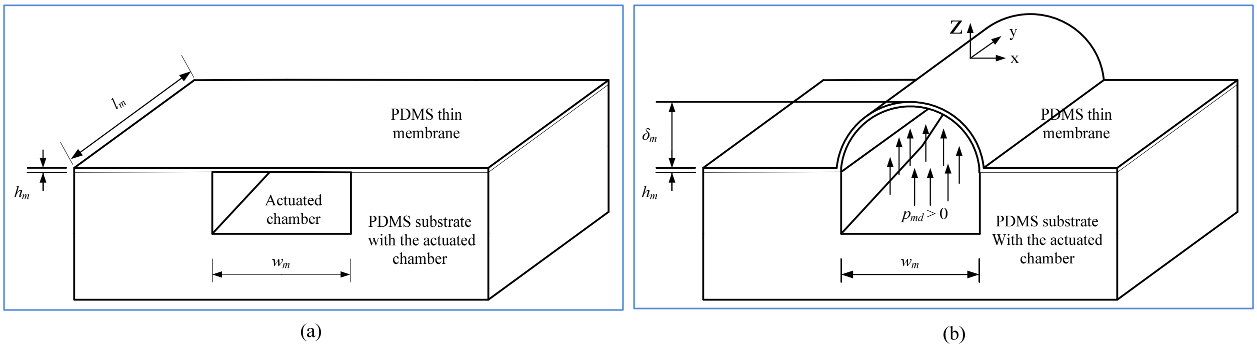

Figure 2. Deformation of the PDMS thin membrane: (**a**) cross-section of the pneumatic microactuator before deformation; (**b**) cross-sectional view of the pneumatic microactuator after deformation.

1. Deformable Force Balance Equation of the PDMS Thin Membrane

When the membrane is subjected to uniformly distributed loads in the Z-direction, it can be assumed that the stresses σ_x, σ_y, τ_{xy}, and τ_{yx} only occur parallel to the middle plane because the membrane is very thin. These stresses do not change with the thickness of the PDMS thin membrane. The normal stresses σ_z perpendicular to the middle plane of the membrane are so small and can be ignored compared with the stresses in the cross-section, that is, $\sigma_z = \tau_{xz} = \tau_{yz} = 0$. The plane stress on each unit width of the membrane is synthesized into the middle plane internal force. The following equations can be obtained [31]:

$$\begin{array}{c} N_x = h_m\sigma_x \;\; N_y = h_m\sigma_y \\ N_{xy} = h_m\tau_{xy} \;\; N_{yx} = h_m\tau_{yx} \end{array} \tag{1}$$

All forces are projected onto the X-axis and Y-axis, and the balance equation can be described as follows:

$$\begin{array}{c} \frac{\partial N_x}{\partial x} + \frac{\partial N_{xy}}{\partial y} = 0 \\ \frac{\partial N_y}{\partial y} + \frac{\partial N_{xy}}{\partial x} = 0 \end{array} \tag{2}$$

The PDMS membrane is in the plane strain state along the Y-direction. The strain, normal stress, and shear stress along the Y-direction will not change due to the force on the membrane. According to Equations (1) and (2), by simplifying and adding the projections of uniform load, transverse shear force, normal force, and tangential force on the Z-axis, which is as follows:

$$p_{md} + \frac{\partial Q_x}{\partial x} + \frac{\partial Q_y}{\partial y} + N_x \frac{\partial^2 \delta}{\partial x^2} = 0 \tag{3}$$

According to Saint–Venant's principle, the transverse shear force per unit width can be found as:

$$\begin{aligned} Q_x &= -D\tfrac{\partial}{\partial x}\nabla^2\delta \\ Q_y &= -D\tfrac{\partial}{\partial y}\nabla^2\delta \end{aligned} \tag{4}$$

According to Equations (3) and (4), the differential equation of elastic surface can be obtained:

$$p_{md} - D\nabla^4\delta + N_x \frac{\partial^2 \delta}{\partial x^2} = 0 \tag{5}$$

According to the definition of bending stiffness, the bending stiffness can be evaluated as below [32]:

$$D = \frac{E_m {h_m}^3}{12(1 - {v_m}^2)} \tag{6}$$

According to the physical properties of PDMS materials, the elastic modulus E_m ~10^5 Pa [33] and the membrane thickness h_m ~10^{-5} m, $12(1 - vm^2)$ ~10^1 can be converted to D ~10^{-11} N·m, so the bending stiffness of the PDMS thin membrane can be neglected.

By adding boundary conditions and transforming Equation (6), the equilibrium equation of the PDMS thin membrane under uniformly distributed load can be described as follows:

$$-p_{md} = \sigma_x h_m \frac{\mathrm{d}^2\delta}{\mathrm{d}x^2} \tag{7}$$

Considering the boundary condition $\delta(\pm w_m/2) = 0$ and Equation (2), and integrating Equation (7), the displacement along the Z-direction can be calculated:

$$\delta = \frac{p_{md}}{2h_m\sigma_x}\left[(w_m/2)^2 - x^2\right] \tag{8}$$

2. Geometric Equation of PDMS Thin Membrane Deformation

The geometric equation of large deflection deformation of the PDMS thin membrane can be described as follows [34]:

$$\begin{aligned} \varepsilon_x &= \tfrac{\partial\varphi}{\partial x} + \tfrac{1}{2}\left(\tfrac{\partial\delta}{dx}\right)^2 \\ \varepsilon_y &= \tfrac{\partial\xi}{\partial y} + \tfrac{1}{2}\left(\tfrac{\partial\delta}{dx}\right)^2 \\ \gamma_{xy} &= \tfrac{\partial\xi}{\partial x} + \tfrac{\partial\varphi}{\partial y} + \tfrac{\partial\delta}{\partial x}\tfrac{\partial\delta}{\partial y} \end{aligned} \tag{9}$$

According to the boundary condition, the first expression of Equation (9) is transformed as follows:

$$\varepsilon_x = \frac{\mathrm{d}\varphi}{dx} + \frac{1}{2}\left(\frac{\mathrm{d}\delta}{dx}\right)^2 \tag{10}$$

3. Physical Equation of PDMS Thin Membrane Deformation

According to the generalized Hooke's law, the physical equation for elastic deformation of the thin membrane can be found as [29]:

$$\begin{aligned} \varepsilon_x &= \tfrac{1}{E_m}(\sigma_x - v_m\sigma_y) \\ \varepsilon_y &= \tfrac{1}{E_m}(\sigma_y - v_m\sigma_x) \\ \gamma_{xy} &= \tfrac{2(1+v_m)}{E_m}\tau_{xy} \end{aligned} \tag{11}$$

The PDMS membrane has a plane strain, and the change in displacement along the Y-direction is 0. According to Equation (11), the stress parallel to the middle plane can be expressed as below:

$$\sigma_y = v_m \sigma_x \tag{12}$$

According to Equations (11) and (12), the stain parallel to the middle plane can be concluded such that:

$$\varepsilon_x = \frac{1 - {\nu_m}^2}{E_m} \sigma_x \tag{13}$$

According to the above equation of the deformation force balance, the geometric equation, and the physical equation of the PDMS thin membrane, the maximum deflection of the PDMS thin membrane is deduced.

According to Equations (10) and (13), it can be concluded that:

$$\frac{\mathrm{d}\varphi}{dx} + \frac{1}{2}\left(\frac{\mathrm{d}\delta}{dx}\right)^2 = \frac{1 - {\nu_m}^2}{E_m} \sigma_x \tag{14}$$

According to Equations (8) and (14), using the boundary condition $\varphi(0) = 0$, the displacement can be obtained such that:

$$\varphi = \frac{1 - {\nu_m}^2}{E_m} \sigma_x x - \frac{1}{6} \frac{{p_{md}}^2 x^3}{(h_m \sigma_x)^2} \tag{15}$$

Using the boundary condition $\varphi(\pm w_m/2) = 0$, the normal stress along the X-direction can be concluded such that:

$$\sigma_x{}^3 = \frac{{p_{md}}^2 E_m (w_m/2)^2}{6{h_m}^2 (1 - {\nu_m}^2)} \tag{16}$$

According to Equation (8), When $x = 0$, the maximum deflection of the PDMS thin membrane can be evaluated as below:

$$\delta_{max} = \frac{p_{md} (w_m/2)^2}{2 h_m \sigma_x} \tag{17}$$

According to Equations (16) and (17), the maximum deflection of the PDMS thin membrane can be obtained:

$$\delta_{\max} = \frac{w_m}{4} \left[\frac{3 p_{md} w_m (1 - {v_m}^2)}{E_m h_m} \right]^{\frac{1}{3}} \tag{18}$$

The PDMS thin membrane is in the plane strain state along the Y-direction. The strain, normal stress, and shear stress along the Y-direction will not change due to the force on the membrane. Simplifying and adding the projections of uniform load, transverse shear force, and normal force. According to the deformation characteristic theory of PDMS and Equation (18), the deformation volume of the PDMS thin membrane can be expressed as below [35]:

$$Vm = \frac{2 l_m w_m \delta_{\max}}{3} \tag{19}$$

3.2. Response Time of the Actuated Microactuator

At a constant step pressure p_s, the actuated chamber is inflated through Orifice 1 of Electromagnetic Microvalve 1. The initial pressure is p_0, and the dynamic pressure of the actuated chamber is p_n. This process must satisfy six assumptions: (1) The permeability of the PDMS material is not considered for a short time during the inflation stage; (2) the working medium N_2 is an ideal air, and potential energy changes are ignored; (3) during the inflation process, there is no macroscopic flow of air in the actuated chamber, and the air change process in the actuated chamber is approximately considered as a quasi-static process; (4) the inflation time is concise, which is regarded as adiabatic inflation; (5) there is sufficient N_2 in the air supply, the constant pressure air supply connected with port S, and its thermodynamic state parameters remain constant; (6) the volume of the actuated pressure fabricated by the PDMS material can be changed and can be subjected to one-dimensional deformation [33,36].

On the basis of the first law of thermodynamics, energy provided by the outside to the actuated chamber is equal to the sum of the total energy change in the actuated chamber and the external work, which can be expressed as [37]:

$$Q_{chem} = E + (i_2 + \frac{1}{2}c_2^2 + gz_2)m_2 - (i_1 + \frac{1}{2}c_1^2 + gz_1)m_1 + W \quad (20)$$

According to the above-mentioned variable-volume actuated chamber filling hypothesis, when the air flows through the valve orifice of Electromagnetic Microvalve 1, the change of the flow parameters with distance is more significant than that with time, which is $\partial/\partial x \gg \partial/\partial t$, and $\partial/\partial t = 0$. The airflow through the valve orifice of Electromagnetic Microvalve 1 should be customarily treated. The cross-sectional area F_s of the S port is much larger than A_p of the throttle port of Electromagnetic Microvalve 1. According to the charging assumption condition (4), the flow process of air through the restrictor orifice S is regarded as an adiabatic flow process.

Convert all variables in Equation (20) into quantities per unit of time, and it can be calculated as:

$$\frac{\mathrm{d}Q_{chem}}{\mathrm{d}t} = \frac{\mathrm{d}E}{\mathrm{d}t} + (i_2 + \frac{1}{2}c_2^2 + gz_2)\frac{\mathrm{d}m_2}{\mathrm{d}t} - (i_1 + \frac{1}{2}c_1^2 + gz_1)\frac{\mathrm{d}m_1}{\mathrm{d}t} + \frac{\mathrm{d}W}{\mathrm{d}t} \quad (21)$$

According to the above conditions, combined with the airflow formula of the electromagnetic microvalve in microscale, where the flow coefficient of the valve port K_{v1} and the microscale correction coefficient before and after the throttle port k_{x1} are constant values, the mass flow of air flowing into the actuated chamber from port S through the intake constraint throttle port S can be expressed as:

$$\frac{\mathrm{d}m_1}{\mathrm{d}t} = k_{x2}k_{v1}k_{x1}A_p\sqrt{\frac{2K}{K-1}} \cdot \frac{p_s}{\sqrt{RT_s}} \cdot \varphi(\varepsilon) \quad (22)$$

where the dimensionless pressure ratio $\varepsilon = p_n/p_s$. The flow resistance flow correction coefficient is generated due to the large area/volume ratio in the microflow channel and the increase in the relative roughness of the pipeline wall, which leads to the rise of internal friction in the fluid flow process and the rise in microscale flow resistance. According to the empirical formula obtained from the test, $k_{x2} = 0.1$ [38].

According to the sixth inflating assumption, it is necessary to linearize the volume change of the actuated chamber. Equation (18) is expanded by the Taylor formula in a small range near the operating point (p_{md0}, δ_{max0}):

$$\delta_{max} = \delta_{max0} + \frac{1}{3}a(p_{md})^{-\frac{2}{3}}|_{p_{md}=p_{md0}}\Delta p_{md} - \frac{\frac{2}{9}a(p_{md})^{-\frac{5}{3}}}{2!}|_{p_{md}=p_{md0}}(\Delta p_{md})^2 + \frac{\frac{10}{27}a(p_{md})^{-\frac{8}{3}}}{3!}|_{p_{md}=p_{md0}}(\Delta p_{md})^3 + \ldots \quad (23)$$

$$a = \frac{w_m}{4}\left[\frac{3w_m(1-{\nu_m}^2)}{E_m h_m}\right]^{\frac{1}{3}} \quad (24)$$

Ignoring terms of higher order above second order, and according to Equations (23) and (24), the maximum deflection pressure gain K_{mp} of the PDMS thin membrane is defined as:

$$K_{mp} = \frac{\Delta\delta_{max}}{\Delta p_{md}} = \frac{1}{3}a(p_{md})^{-\frac{2}{3}} \quad (25)$$

K_{mp} represents the maximum deflection variation caused by the unit pressure applied on the PDMS thin membrane. The greater the gain, the more sensitive the control of the deflection of the PDMS thin membrane.

The variable-air capacity has no leakage, and the kinetic energy and potential energy changes of the air entering the variable-air chamber are ignored. Because it is assumed that the air in the actuated chamber has no visible flow and is approximately considered to be quasi-static, the macroscopic kinetic energy of the system is zero, and the increment of the macroscopic kinetic energy can be given as below:

$$\frac{\mathrm{d}E}{\mathrm{d}t} = \frac{\mathrm{d}(mu)}{\mathrm{d}t} \tag{26}$$

where u, c_v, K, and R can be calculated as the following formulas:

$$\begin{gathered} u = c_v \cdot T,\ \ c_v = \tfrac{R}{K-1},\ \ p_n V_c = mRT, \\ K = \tfrac{c_p}{c_v},\ \ R = c_p - c_v \\ \mathrm{d}(p_n V_c) = p_n \mathrm{d}V_c + V_c \mathrm{d}p_n \end{gathered} \tag{27}$$

Consequently, the increment of specific internal energy in the actuated chamber can be given as:

$$\frac{\mathrm{d}(mu)}{\mathrm{d}t} = \frac{1}{K-1}(p_n \frac{\mathrm{d}V_c}{\mathrm{d}t} + V \frac{\mathrm{d}p_n}{\mathrm{d}t}) \tag{28}$$

Adiabatic inflation and the system can be calculated as below:

$$\frac{\mathrm{d}Q_{chem}}{\mathrm{d}t} = 0 \tag{29}$$

Stagnation enthalpy of N_2 per unit mass in tube S can be calculated as the following formulas:

$$i_1 = \frac{a_{s^*}^2}{K-1},\ \ a_{s^*}^2 = KRT_1,\ \ T_1 = T_s \tag{30}$$

By transforming the above Equation (30), stagnation enthalpy i_1 can be found as:

$$i_1 = \frac{KRT_s}{K-1} \tag{31}$$

The external expansion work of the working medium N_2 in the actuated chamber can be given as below:

$$\frac{\mathrm{d}W}{\mathrm{d}t} = p_n \cdot \frac{\mathrm{d}V}{\mathrm{d}t} \tag{32}$$

According to Equations (21), (26), and (29), the transformation can be obtained as follows:

$$i_1 \cdot \frac{\mathrm{d}m_1}{\mathrm{d}t} = \frac{\mathrm{d}(mu)}{\mathrm{d}t} + \frac{\mathrm{d}W}{\mathrm{d}t} \tag{33}$$

According to Equations (28) and (31)–(33), the change of N_2 pressure p_n in any instantaneous actuated chamber with inflation time t can be expressed as follows:

$$\frac{\mathrm{d}p_n}{\mathrm{d}t} = \frac{KRT_s}{V_c} \cdot \frac{\mathrm{d}m_1}{\mathrm{d}t} - \frac{Kp_n}{V_c}\frac{\mathrm{d}V_c}{\mathrm{d}t} \tag{34}$$

According to Equations (22) and (34), the air pressure in the actuated chamber with variable volume is inflated with constant pressure p_s. When the air pressure in the actuated chamber is increased from the initial pressure p_0 to the pressure p_n ($p_n \le p_s$), the relationship is as follows:

$$\frac{\mathrm{d}p_n}{\mathrm{d}t} = \frac{Kk_{x2}k_{v1}k_{x1}A_p\sqrt{\frac{2K}{K-1}}\sqrt{RT_s}}{V_c} p_s \varphi(\frac{p_n}{p_s}) - \frac{Kp_n}{V_c}\frac{\mathrm{d}V_c}{\mathrm{d}t} \tag{35}$$

According to Equations (34) and (35), c_1, c_2, and c_3 are all coefficients and can be expressed as follows:

$$c_1 = Kk_{x2}k_{v1}k_{x1}A_p\sqrt{\frac{2K}{K-1}}\sqrt{RT_s}p_s \tag{36}$$

$$c_2 = \frac{2l_m w_m}{3}\cdot K_{mp},\ \ c_3 = \mathrm{a}\frac{2l_m w_m}{3}K_{mp}p_{md} \tag{37}$$

The air pressure increment of the actuated chamber can be expressed as:

$$\frac{\mathrm{d}p_n}{\mathrm{d}t} = \frac{c_1\varphi(\varepsilon)}{V_0+V_m} - \frac{Kp_n}{V_0+V_m}c_2\frac{\mathrm{d}p_n}{\mathrm{d}t} \tag{38}$$

c_2 and c_3 are both coefficients. By transforming Equation (38), the inflatable time increment, c_2 and c_3 can be calculated as follows:

$$\mathrm{d}t = \frac{c_4}{\varphi(\varepsilon)}\mathrm{d}\varepsilon + \frac{c_5}{\varphi(\varepsilon)}\varepsilon\mathrm{d}\varepsilon \tag{39}$$

$$c_4 = \frac{(V_0+c_3)p_s}{c_1},\ \ c_5 = \frac{(1+K)c_2{p_s}^2}{c_1} \tag{40}$$

ε^* = 0.528 is the critical pressure ratio between the upper and downstream of the valve port. When $\varepsilon \le \varepsilon^*$, the air flows at the speed of sound, the flow rate of the electromagnetic microvalve reaches the maximum, and the decrease of the downstream pressure will not make the mass flow increase again, the phenomenon of "congestion". When $\varepsilon > \varepsilon^*$, the air flows at subsonic speed, and the air mass flow rate through the valve port is not only related to the effective flow area of the valve port but also related to the upper and downstream pressure of the valve port [39]:

$$\varphi(\varepsilon) = \begin{cases} \sqrt{\frac{(K-1)}{2}\left(\frac{2}{K+1}\right)^{(K+1)/(K-1)}} & \varepsilon \le \varepsilon^* \\ \sqrt{\varepsilon^{2/K} - \varepsilon^{(K+1)/K}} & \varepsilon > \varepsilon^* \end{cases} \tag{41}$$

When $\varepsilon = p_n/p_s \le 0.528$, that is, when the inflation is sonic inflow, substituting Equation (41) into Equation (39) and integrating, the inflation time can be expressed as below:

$$t_\mathrm{I} = c_6[(p_n/p_s) - (p_0/p_s)] + c_7[(p_n/p_s)^2 - (p_0/p_s)^2] \tag{42}$$

$$c_6 = c_4/\varphi(\varepsilon),\ \ c_7 = c_5/2\varphi(\varepsilon) \tag{43}$$

When $\varepsilon = p_n/p_s > 0.528$, the inflation is subsonic inflow, substituting Equation (41) into Equation (39). Their equations can be given as:

$$t_{\mathrm{II}} = c_6{}'[\sqrt{1-(p_0/p_s)^{(K-1)/K}} - \sqrt{1-(p_n/p_s)^{(K-1)/K}}] + c_7{}'\int_{z_2}^{z_1}(1-z^2)^{K/(K-1)}\mathrm{d}z \tag{44}$$

$$c_6{}' = \frac{2K}{K-1}c_4,\ \ c_7{}' = \frac{2K}{K-1}c_5 \tag{45}$$

$$z = \sqrt{1-\varepsilon^{(K-1)/K}} \tag{46}$$

Expanding and summing the second item on the right of Equation (44) according to the Taylor formula, one can obtain:

$$\int_{z_2}^{z_1}(1-z^2)^{K/(K-1)}\mathrm{d}z = [z + (-2)\frac{1}{3!}\alpha z^3 + (-2)^2\frac{1\times 3}{5!}\alpha(\alpha-1)z^5 + \ (-2)^3\frac{1\times 3\times 5}{7!}\alpha(\alpha-1)(\alpha-2)z^7 + \ldots]_{z_2}^{z_1} \tag{47}$$

$$z_1 = \sqrt{1-\left(\frac{p_0}{p_s}\right)^{(K-1)/K}},\ \ z_2 = \sqrt{1-\left(\frac{p_n}{p_s}\right)^{(K-1)/K}} \tag{48}$$

$$\alpha = \frac{K}{K-1} \tag{49}$$

The time of inflating the actuated chamber from the initial pressure p_0 to the pressure p_n ($p_n \leq p_s$) is calculated in two stages: In the first stage, the air source pressure p_s and initial pressure p_0 are inflated the actuated chamber to p_{sub}, p_{sub}/p_s = 0.528, and the charging time t_{I} is calculated according to Equation (42). In the second stage, the air source pressure p_s is inflated, the initial pressure is p_{sub}, and the charging time t_{II} is calculated according to Equations (44) and (47). Then, the sum inflating time is the total actuated chamber filling time, $t = t_{\mathrm{I}} + t_{\mathrm{II}}$.

It is noted that the initial pressure of the actuated chamber p_0 is the ambient pressure. When $p_0/p_s \leq 0.528$, the inflation is sonic inflow, that is, $p_s \geq p_0/0.528$, and the absolute pressure of the air source $p_s \geq 191$ kPa is calculated. Therefore, when the absolute pressure of air source p_s is lower than 191 kPa, the whole inflation process is subsonic inflow. When the absolute pressure of the air source is greater than 191 kPa, and the final charging pressure of the actuated chamber p_n is greater than 191 kPa, the initial pressure to p_{sub} in the first stage of inflation is sonic inflow, p_{sub} = 0.528 p_s; The initial pressure of the second stage of inflation is p_{sub}, and when it is inflated to p_n, it is subsonic inflow.

4. Results and Discussions

The PDMS thin membrane is spin-coated on the silicon wafer by a spin coater at 1500 r/min, and the ratio of the prepolymer solution (base/curing agent) is 15:1 of Sylgard 184. The ratio of the prepolymer solution is 8:1 of Sylgard 184 of the PDMS substrate with a microchannel for better plasticity. Detailed information about the fabrication process of the PDMS thin membrane and the micromixer can be found in our previous study [40]. To simplify the aerodynamic microactuator model, the air permeability of the PDMS material and the flow channel deformation due to pressure are ignored. The PDMS components include the PDMS thin membrane, the PDMS microactuator, the on-chip microvalve, and the mixer. Because of the manufacturing error, the design values of the parameters are not exactly the same as the actual values used in the experiment.

4.1. Analysis of Deformation Characteristics of PDMS Thin Membrane

The PDMS actuated membrane is the driving component of pneumatic microfluidic, and its shape is shown in Figure 3a. According to the previous analysis, the PDMS thin membrane is a double-symmetric structure, and 1/4 part of the model is used as the analysis object. By adding symmetric constraints, the effect of partial modeling can be realized to replace the entire model, reducing the amount of calculation. The density of the grid determines the accuracy of the computation, but it also determines the amount of computation and how much time it takes. At the initial state and after the deformation, the residual stress is 0, and the model structure adopts the peripheral fixed support. To strike a balance between the calculation accuracy and the calculation amount, the mesh density of the deformed part of the PDMS-driven membrane is four times that of other areas, and the quadratic tetrahedral mesh partition model is adopted. A total of 58,042 meshes are introduced into the calculation, as shown in Figure 3b. Figure 3c is the finite element deformation cloud diagram of the PDMS thin membrane when the uniform pressure is 80 kPa, and its deformation shape is similar to the trajectory of the parabolic function. Using the ANSYS simulation software and the project module loop function, the deflection of the PDMS thin membrane under different uniform distribution pressures is obtained.

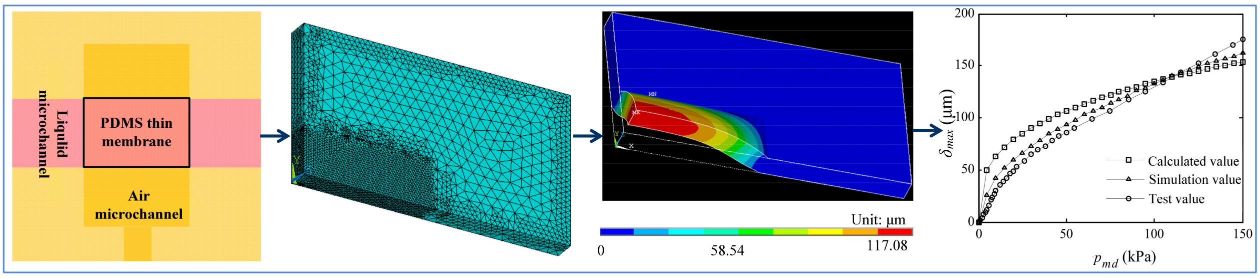

(a) (b) (c) (d)

Figure 3. Deformation of the PDMS actuated membrane with 500 μm × 200 μm × 40 μm: (**a**) shape of the PDMS actuated membrane; (**b**) FEM model meshing; (**c**) deformation with 80 kPa; (**d**) comparison of maximum deflection results.

A laser displacement sensor (Keyence, LK-G5000) is used to measure the maximum deflection of the PDMS thin membrane of the pneumatic microactuator. In the measurement test of the maximum deflection of the PDMS thin membrane under uniform pressure, the air pressure in the actuated chamber should increase slowly from small to large, because the pressure amplitude increasing too fast will cause the inaccurate measurement or the collapse of the actuated chamber. Figure 3d is the comparison among the theoretical calculation data, the finite element simulation results, and the test values of the maximum deformation of the PDMS thin membrane under different uniformly distributed pressures. The finite element simulation results are similar to the exponential curve relationship and accord with the significant deformation behavior of PDMS nonlinear high-elastic materials. In the initial stage, when the consistent pressure p_{md} is less than 120 kPa, the finite element value is slightly less than the theoretical calculation result. With the increase of uniform pressure, when p_{md} is more than 120 kPa, the finite element calculation value is larger than the theoretical calculation result. The comparison result shows that the nonlinearity slope of the curves is different. Because the simulation process mainly considers the mechanical properties of the PDMS thin membrane of super elastic and large deformation. Theoretical curves have a more significant mean curvature because the derivation formula has certain unreliability. The distinction in the nonlinearity of the curves is similar to the comparison curves, and there is an approximate cause analysis in Reference [41]. From the calculation and simulation results, when the uniform pressure is close to zero, the curves are nonlinear, so the experimental data collection is relatively dense to fit the experimental curve. The latter part of the curves of the calculation and simulation results are simple linear, so a large sampling interval of experimental data collection can be selected. Although there is a particular deviation among the theoretical calculation results, the finite element simulation results, and test data, the overall variation trend of the three results is consistent, indicating that the previous theoretical analysis is in line with the actual situation, which is used to understand and analyze the deformation phenomenon of rectangular PDMS thin membrane. Furthermore, the experimental results can verify the correctness of the theoretical analysis and finite element calculation.

4.2. Dynamic Response Performance of the Pneumatic Microactuator

The pneumatic microactuator transforms the electric energy of the off-chip pneumatic control microvalve and the pressure energy of the air source into the mechanical energy of the membrane driven by the membrane microvalve PDMS. The response process involves electric power, hydraulic energy, and mechanical energy, which is a multiphysical field coupling process. Figure 4a describes each operation step and model for the actuator system. During the inflation process of the pneumatic microactuator, the working medium N_2 is diatomic air, the adiabatic exponent is 1.41, the air constant is 287 J/Kg·k, and the air supply temperature is 287 k (about 15 °C). The outside pressure and the initial pressure p_0 in the actuated chamber are ambient pressure, p_0 and p_l are both 1.01×10^5 Pa. In this paper, the response time of the pneumatic actuator is mainly studied, and the gas flow state in the valve chamber is not considered, so the compressibility of the gas is ignored. Except for the elastic actuated chamber part, the deformation effect of the PDMS microchannel in the working process is not considered. There is no slip at the boundary. In specific applications, such as the pneumatic microactuator as the driving device of the membrane microvalve, p_l should take the pressure of the liquid working medium in the upper liquid microchannel on the PDMS thin membrane.

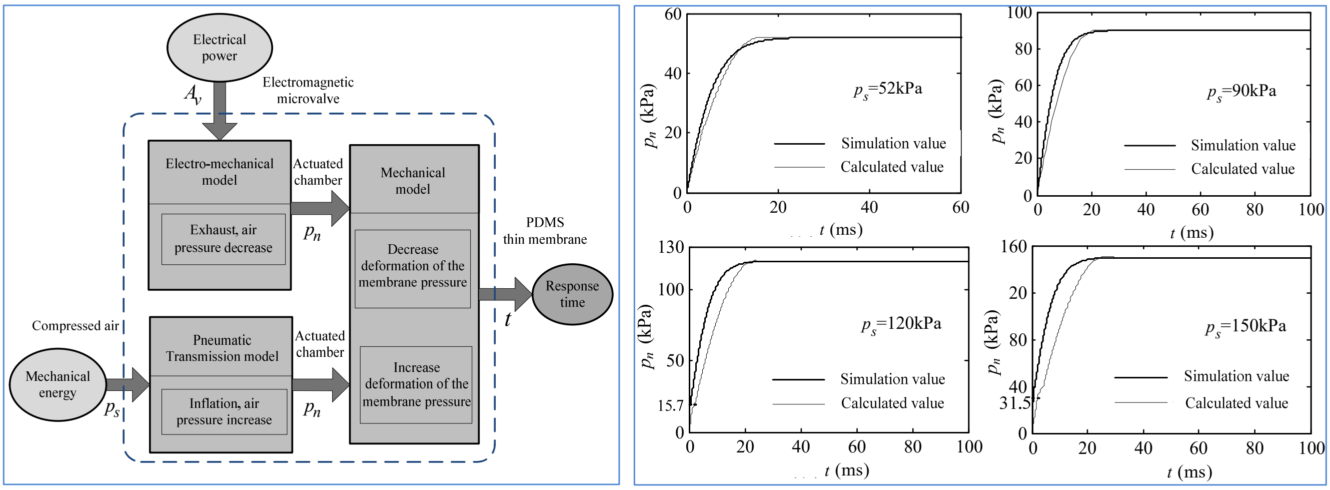

(a) (b)

Figure 4. System model and response characteristics of the pneumatic microactuator: (**a**) operational steps and system model; (**b**) response time with different p_s.

The relaxation time of PDMS material itself affects the response time of the system to a certain extent. Adjusting the crosslinking density by controlling the mixing ratio of the prepolymer is an effective method to change the microstructure and elastic modulus of PDMS, thus changing the relaxation time of the material. In this paper, the elastic modulus of PDMS is 550 kPa, and its relaxation time should be less than 10 µs. Therefore, the influence of PDMS relaxation time is ignored [42]. When the relaxation time of the PDMS itself is not considered, the actuated time is equal to the recovery time of the pneumatic microactuator. In the actual working process, the change of valve port pressure difference is always coupled with the evolution of air resistance, which jointly affects the dynamic performance of the pneumatic microactuator.

Figure 4b shows the pressure dynamic response characteristic curve of the pneumatic microactuator when the opening of Electromagnetic Microvalve 1 is 20%, and the actuated chamber is inflated to the air source pressure. The higher the charging pressure of the actuated chamber, the longer the charging response time of the pneumatic microactuator is. As can be seen from the figure, when the air source pressure p_s = 52 kPa, the actuated chamber is inflated to the pressure value, and the simulation inflation time is t = 14.79 ms. When p_s = 90 kPa, the inflation time is t = 20.11 ms. When p_s = 120 kPa, the inflation time is t = 23.12 ms. When p_s = 150 kPa, the inflation time is t = 25.28 ms. According to the pneumatic microactuator inflation mathematical model, when the air supply pressure is higher than 90 kPa, the initial phase of air volume inflation is sonic inflation. According to the response curve, when the air source pressure is 120 kPa and 150 kPa, the response curve has prominent segments (as shown by the dotted line in the figure), and the pressure value of the segment point is 15.7 kPa and 31.5 kPa, respectively. Moreover, the curve slope before the segment point is significantly higher than that after the segment point. It indicates that the inflation rate before the segment point is higher than after the segment point. It also indicates that the inflation process before the segmented point belongs to sonic inflation. In contrast, the inflation process after the segmented point belongs to subsonic inflation, which is consistent with the mathematical model of the elastic air volume. The response time is higher than a similar type of pneumatic actuator [43,44].

From the above analysis, it can be concluded that the main factors affecting the response time of the pneumatic microactuator include air source pressure, off-chip electromagnetic microvalve throttle, and air capacity. The system resistance is mainly determined by the electromagnetic microvalve opening γ_e. The size of the valve opening γ_e is also used to control the actuated chamber inlet and exhaust flow.

4.3. Response Characteristics Analysis of Membrane Microvalve Integrated with the Microactuator

The valve control technology of the on-chip membrane microvalve on liquid flow is a core technology of a microfluidic system. The cross-section of the liquid microchannel shows a parabolic trajectory, and the deflection result of the PDMS thin membrane is also approximately parabolic trajectory. Figure 5a shows the schematic diagram of the opening of the membrane microvalve under different driving pressures.

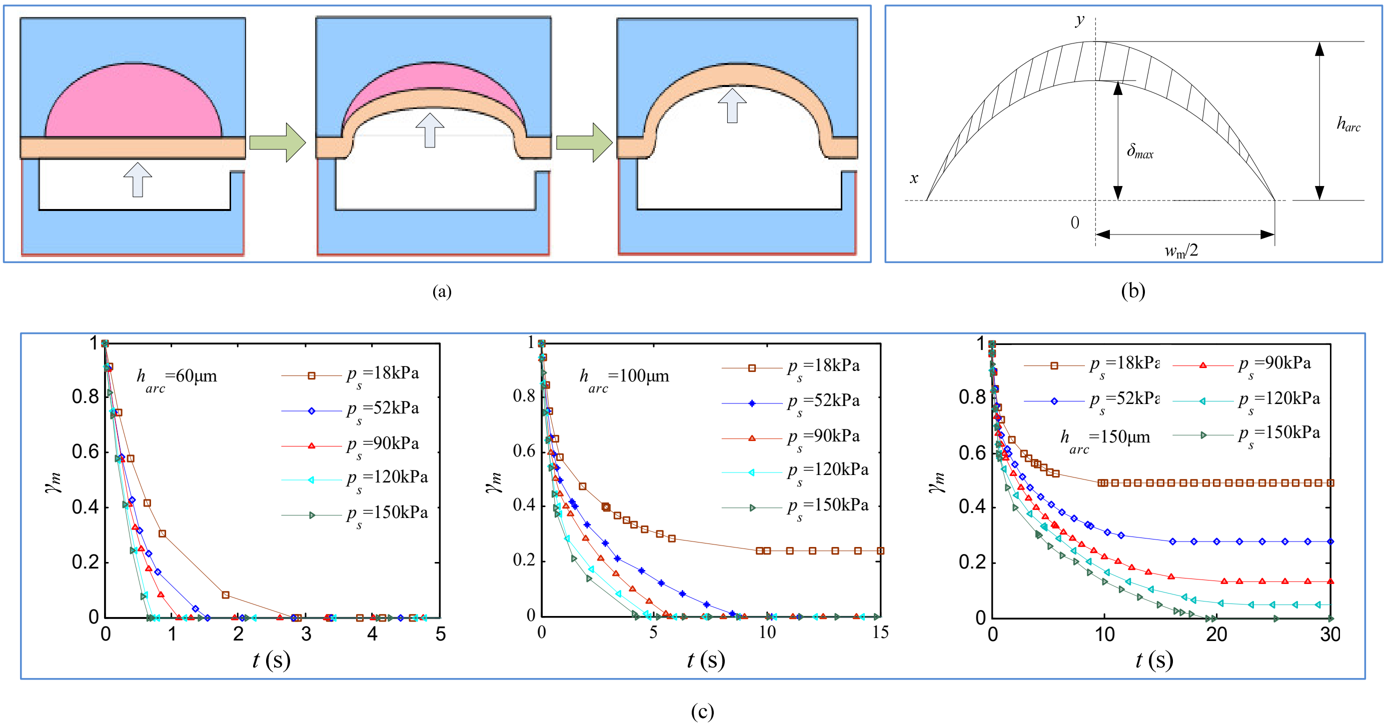

Figure 5. Schematic diagrams of the valve opening γ_m and simulation results of response about the membrane microvalve: (**a**) valve port from open to close state; (**b**) size of the valve port: (**c**) simulation results of γ_m with different t.

Assume that the depth of the liquid arc microchannel is h_{arc}, the width of the microchannel is the width w_m before the deformation of the PDMS thin membrane, the maximum deflection of the PDMS thin membrane deformation is δ_{max}, and the opening of the membrane microvalve is $\gamma_m = (h_{arc} - \delta_{max})/h_{arc}$, as shown in Figure 5b. The shaded area in the figure represents the effective throttling area of the on-chip membrane microvalve. By subtracting the deformation area of the PDMS thin membrane from the fully open area of the valve port, the valve port space of the membrane microvalve with different valve port opening degrees can be obtained: $A_m = A_0 - A_{mem}$. According to the Newton-Leibniz integral formula, the parabolic area is obtained: $A_m = 2/3w_m(h_{arc} - \delta_{max})$. According to the aforementioned dynamic response characteristics of the pneumatic microactuator, when the depth h_{arc} of the liquid microchannel on-chip membrane microvalve is constant, the larger the opening of the membrane microvalve port, the shorter the response time. The valve opening degree of Electromagnetic Microvalve 1 is 20%, and Electromagnetic Microvalve

2 is closed. When the liquid microchannel depth h_{arc} is 60 µm, 100 µm, and 150 µm, the relationship between the membrane microvalve port opening γ_m and the response time t is shown in Figure 5c. The simulation response time values of the membrane microvalve and the associated design parameters are presented in Table 2.

Table 2. Simulation response time values of the membrane microvalve and the associated design parameters.

h_{arc} (µm)	p_s (kPa)	δ_{max} (µm)	γ_m	t (ms)
60	18	60	0%	2.84
	52	60	0%	1.54
	90	60	0%	1.11
	120	60	0%	0.74
	150	60	0%	0.66
100	18	76	24%	-
	52	100	0%	8.81
	90	100	0%	5.70
	120	100	0%	4.78
	150	100	0%	4.26
150	18	76	49%	-
	52	108.24	28%	-
	90	129.96	13%	-
	120	143.04	5%	-
	150	-	0%	19.18

4.4. Experimental Operation of Valving and Mixing Integrated with the Microactuator

The microvalve comprises the sample layer located upper with a liquid channel and the control layer located bottom with the pneumatic microactuator. The two-dimensional and three-dimensional schematics of the microvalve integrated with the pneumatic microactuator are shown in Figure 6a. The pneumatic micromixer is constituted of the mixing chamber located upper and the actuated microactuator located bottom. By controlling the pressure change in the pneumatic microactuator, the operation of the pneumatic micromixer is controlled. The mixing principle and the encapsulated pneumatic micromixer are shown in Figure 6b.

The fluid driving setup of the experimental system for valving and mixing includes a compressed gas source, two sets of pressure regulating devices, and a gas–liquid acting vessel, as shown in Figure 6c. The compressed air source is integrated with an air filter to ensure the gas medium is clean and dry. In the pneumatic-driven liquid flow system, one air path can accurately control the pressure of the liquid microchannel of the pneumatic microfluidic chip, to accurately control the liquid flow, and the other air path is connected with the gas microchannel of the pneumatic microfluidic chip to achieve accurate control of the driving pressure. The pneumatic-driven liquid flow system can not only achieve a fast response but also realize multiple liquid or air parallel drives when equipped with numerous pressureregulating devices.

The valving results under different actuated pressures are observed, as shown in Figure 6d. The liquid layer is filled with a red sample, and the microvalve area is marked with a dashed box. The color depth in the dashed line area means the size of the valve opening, and the color depth represents the large thickness of the liquid layer and the large valve opening. The light color represents the liquid layer is shallow, and the valve opening is small. Colorless means that the fluid flow is completely blocked, and the microvalve is completely closed. The valve opening of the membrane valve is determined by the pressure of the pneumatic microactuator. The package geometry of the pneumatic actuator is 297 µm × 489 µm × 100 µm, and the width and the depth of the liquid channel are 276 µm and 78 µm, respectively. The air pressures of the pneumatic microactuator are from 0 to 120 kPa in 10 kPa increments. The width of the closed microvalve is larger with increasing actuated pressure. The microvalve starts in the fully closed state when the actuated air pressure equals 70 kPa. It is important to notice that the working pressure of the proposed actuator should not exceed 280 kPa, which is the pressure that the PDMS seal strength can withstand. If it exceeds this value, the body of the PDMS actuator may burst open through repeated experiments.

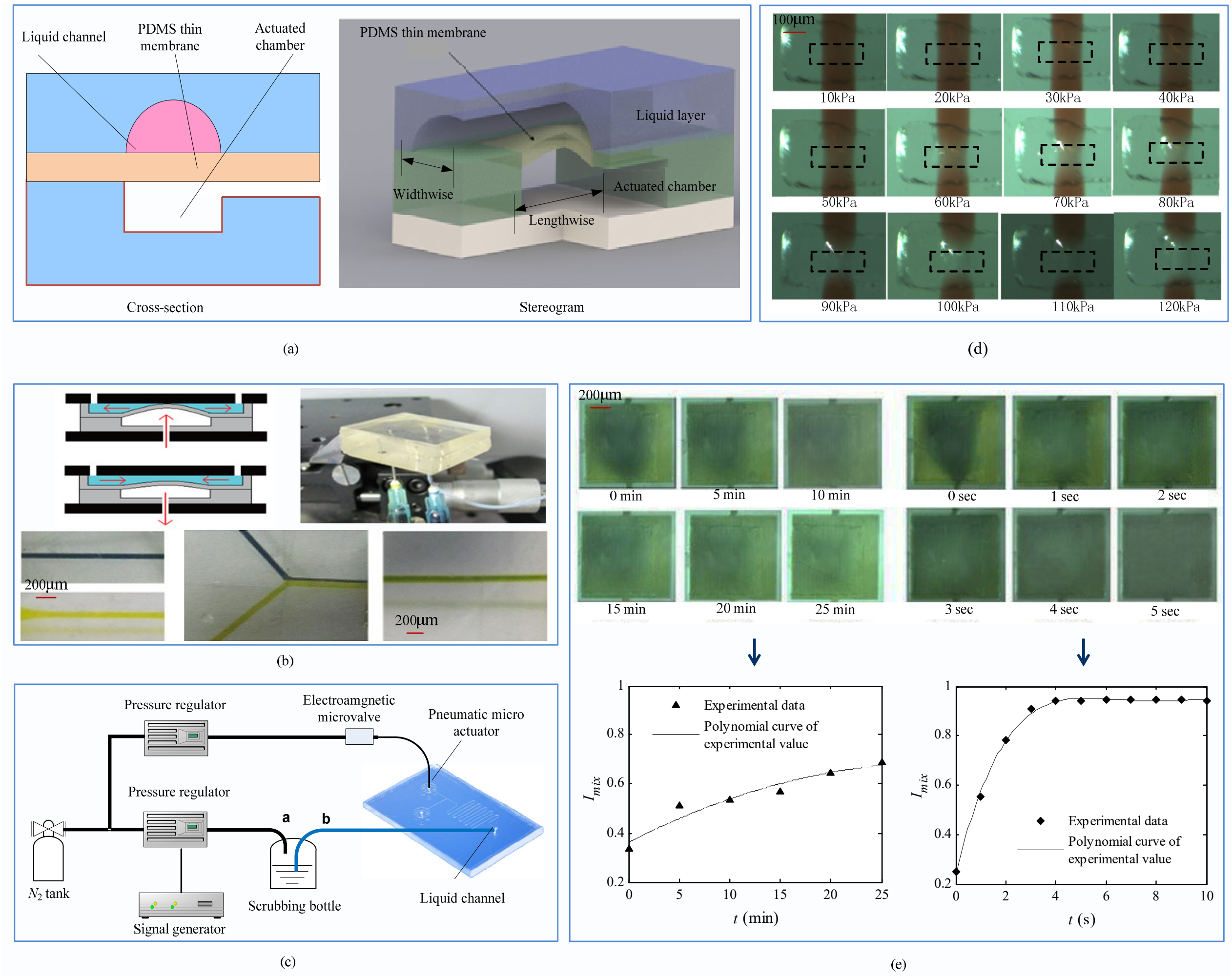

Figure 6. Schematic diagrams of the valve opening γ_m and simulation results of response about the membrane microvalve: (**a**) schematic diagram of on-chip membrane microvalve; (**b**) motion of the PDMS actuated membrane and reagents of the micromixing chamber in a cycle and the packaged pneumatic micromixing chip; (**c**) schematic diagram of a pressure drive device for the experimental system; (**d**) microscope images of the membrane microvalve with different γ_m; (**e**) microscope photos and mixing results comparison of reagents caused by natural convection and the pneumatic microactuator.

The design size of the upper liquid micromixing chamber is 1.0 mm × 1.0 mm × 0.1 mm, and the size of the lower driving chamber is 0.8 mm × 0.8 mm × 0.1 mm. The center of the micromixing chamber and the driving chamber are overlapped in space, and the middle layer is a PDMS driving membrane with a thickness of 40 μm. A certain proportion of yellow and blue reagents are filled into the micromixing chamber of the micromixer. Figure 6e shows the microscope photos and mixing results comparison of reagents caused by free convection and the microactuator. The vibration mixing mode is adopted, the pressure of the driving cavity is 20 kPa, and the vibration frequency of the pneumatic micromixer is set to 1 Hz. The quantified mixing efficiency of different color reagents based on the digital image RGB color model, gray conversion model, and variance equation [45,46] is shown and corresponds to those samples blending pictures. The mixing efficiency by free convection is only 68.75% after 25 min due to slower molecular diffusivity under microscale, and the experimental results show that the mixing efficiency by the pneumatic microactuator is as high as 94% after mixing for 5 s, and it is almost completely mixed. Compared with similar studies, the micromixer with integrated the proposed pneumatic microactuator has a shorter mixing time and higher mixing efficiency [47,48]. It is noted that, according to the results of repeated experiments, the vibration frequency of the micromixer is not higher than 10 Hz because of the large air resistance caused by the small cross-sectional area of the microchannel, if the vibration frequency is too high, the air pressure in the actuated chamber is too late to inflate or release, resulting lower mixing efficiency. In addition, the driving pressure should not be greater than 30 kPa, because the maximum deflection of the PDMS membrane is greater than the depth of the mixing chamber. The influence of excess driving displacement of the PDMS membrane on the mixing efficiency is negligible.

5. Conclusions

To predict the pneumatic microfluidic chip response time, the structure and working principle of the pneumatic microactuator are given, and its dynamic response mathematical and numerical simulation models are established. The maximum deflection of the PDMS actuated membrane, the pressure of the actuated chamber, the volume of the actuated chamber, and the response time under different valve openings of the on-chip membrane microvalve are studied by theory, simulation, and experimental methods. The mathematical model and simulation results show that when the pressure of the air source is 120 kPa and 150 kPa, the response curve has obvious segments, and the pressure value of the segment point is 15.7 kpa and 31.5 kpa, respectively. This indicated that the inflation process before the segmented point belongs to sonic inflation, and the inflation process after the segmented point belongs to subsonic inflation. The geometric size of the microchannel (air resistance), the air pressure of the actuated chamber, and the volume of the actuated chamber are multiphysical field coupling systems, and their interactions jointly determine the response characteristics of the pneumatic microactuator. The simulation results show that when the liquid microchannel depth is 60 μm and the air source pressure is 18 kPa and 150 kPa, it takes 2.84 ms and 0.66 ms to completely close the on-chip membrane valve, respectively. Liquid sample valving and mixing performances are experimented to assess the performance of the pneumatic microactuator. The experimental results showed that the mixing efficiency of the two color reagents is 94% at 5 s, and the mixing time is less than other pneumatic methods, which meets most mixing requirements at microscales. According to the results of repeated experiments, there are some limitations to the proposed PDMS pneumatic microactuator and the designed micromixer. The working pressure of the proposed actuator should not exceed 280 kPa; otherwise, the PDMS body of the pneumatic microactuator may burst open. In addition, the vibration frequency of the micromixer should not be higher than 10 Hz, and the driving pressure should not be greater than 30 kPa.

The dynamic response model of the pneumatic microactuator proposed in this paper can be used to help further develop the on-chip microvalve technology and the control and actuation of this type of microactuator. This research provides a theoretical basis for predicting the response time of pneumatic chips in biological and chemical applications, which can promote the application of pneumatic microfluidic chip research and development of high-integration pneumatic microfluidic chip intelligent application systems such as molecular detection and disease diagnosis, meet the huge market demand for new intelligent pneumatic microfluidic chip applications. It is of great practical significance to promote global portable microfluidic technology products. Future work needs to be conducted to optimize the size of the actuated membrane and the geometries of the actuated chamber, and to study the multiphysics coupling mechanism during the actuated process inside the microchannel. Obtaining precisely actuated pressures and driving frequency is of great significance for further improving the actuated efficiency of pneumatic microsystems.

Author Contributions: Conceptualization, S.L.; methodology, G.Y.; software, S.J.; formal analysis, W.Z.; data curation, H.S.; writing—original draft preparation, X.L.; writing—review and editing, X.L.; project administration, L.W.; funding acquisition, X.L., H.S. and L.W. All authors have read and agreed to the published version of the manuscript.

Funding: This research was funded by the National Natural Science Foundation of China (No.: 52005453 and 52075500), the Key Science and Technology Research Project of the Henan Province (No.: 222102310213), and the Science and Technology Project of the Henan Provincial Department of Transportation (No.: 2020J2).

Data Availability Statement: The data presented in this study are available on request from the corresponding author.

Conflicts of Interest: There are no conflicts of interest to declare.

Nomenclature

δ_{max}	maximum deflection of membrane, μm	gz_1	potential energy flowing into actuated chamber, J/N
p_n	air pressure of actuated chamber, Pa	gz_2	potential energy flowing out of actuated chamber, J/N
p_l	liquid pressure on membrane, Pa	p_s	air pressure of air supply, Pa
E_m	elastic modulus, kPa	p_0	initial air pressure of actuated chamber, Pa
v_m	Poisson ratio	F_s	cross-sectional area of port S, m^2
V_m	volume of actuated chamber, m^3	A_p	Electromagnetic Microvalve 1 cross-sectional area, m^2
l_m	length of thin PDMS membrane, m	k_{v1}	valve port flow coefficient
w_m	width of thin PDMS membrane, m	k_{x1}	correction factor
t_m	thickness of thin PDMS membrane, m	k_{x2}	flow resistance flow correction factor
E	tonal energy of the actuated chamber, J	Δp_{md}	p_{md} incremental in a small range, Pa
l_0	length of air channel, m	$\Delta\delta_{max}$	incremental maximum deflection, μm
w_0	width of air channel, m	K_{mp}	maximum deflection—pressure gain
h_0	depth of the air channel, m	t	Time, s
l_a	length of actuated chamber, m	u	fluid thermal conductivity, W m^{-1} K^{-1}
w_a	width of actuated chamber, m	R	air constant, J/(mol·K)
h_a	depth of actuated chamber, m	c_p	specific heat at constant pressure, J/(kg·K)
m_1	mass flow rate flowing into actuated chamber, kg/s	c_v	specific heat at constant volume, J/(kg·K)
m_2	mass flow rate flowing from the actuated chamber, kg/s	V_0	initial volume of actuated chamber, m^3
A_m	Valve port area of membrane microvalve, m^2	V_m	increase volume of actuated chamber, m^3
A_0	Valve port area with fully opened, m^2	h_{arc}	depth of curved liquid microchannel, m
A_{mem}	deformation area of PDMS thin membrane, m^2	γ_m	Valve opening of membrane microvalve
W	work of N_2 in actuated chamber, J	$1/2{c_1}^2$	kinetic energy flowing out of actuated chamber, J/m^2
i_1	enthalpy flowing into actuated chamber, J/kg	$1/2{c_1}^2$	kinetic energy flowing into actuated chamber, J/m^2
i_2	enthalpy flowing out actuated chamber, J/kg	p_{sub}	air pressure cut-off point, Pa

References

1. Zheng, D.; Wang, Z.; Wu, J.; Li, S.; Li, W.; Zhang, H.; Xia, L. A raman immunosensor based on SERS and microfluidic chip for all-fiber detection of brain natriuretic peptide. *Infrared Phys. Technol.* **2022**, *125*, 104252. [CrossRef]
2. Sjoberg, R.G.; Leyrat, A.A.; Pirone, D.M.; Chen, C.S.; Quake, S.R. Versatile, fully automated, microfluidic cell culture system. *Anal. Chem.* **2007**, *79*, 8557–8563. [CrossRef] [PubMed]
3. Guan, Y.; Yang, T.; Wu, J. Mixing and transport enhancement in microchannels by electrokinetic flows with charged surface heterogeneity. *Phys. Fluids* **2021**, *33*, 042006. [CrossRef]
4. Yang, T.; Peng, J.; Shu, Z.; Shu, Z.; Sekar, P.K.; Li, S. Determination of the membrane transport properties of jurkat cells with a microfluidic device. *Micromachines* **2019**, *10*, 832. [CrossRef] [PubMed]
5. Jiang, B.; Guo, H.; Chen, D.; Zhou, M. Microscale investigation on the wettability and bonding mechanism of oxygen plasma-treated PDMS microfluidic chip. *Appl. Surf. Sci.* **2022**, *574*, 151704. [CrossRef]
6. Chen, S.; Sun, Y.; Fan, F.; Chen, S.; Zhang, Y.; Zhang, Y.; Meng, X.; Lin, J.-M. Present status of microfluidic PCR chip in nucleic acid detection and future perspective. *TrAC Trends Anal. Chem.* **2022**, *157*, 116737. [CrossRef]

7. Araci, I.E.; Agaoglu, S.; Lee, J.Y.; Yepes, L.R.; Diep, P.; Martini, M.; Schmidt, A. Flow stabilization in wearable microfluidic sensors enables noise suppression. *Lab Chip* **2019**, *19*, 3899–3908. [CrossRef]
8. Araci, I.E.; Quake, S.R. Microfluidic very large scale integration (mVLSI) with integrated micromechanical valves. *Lab Chip* **2012**, *12*, 2803–2806. [CrossRef]
9. Whitesides, G.M. The origins and the future of microfluidics. *Nature* **2006**, *442*, 368–373. [CrossRef]
10. ESackmann, K.; Fulton, A.L.; Beebe, D.J. The present and future role of microfluidics in biomedical research. *Nature* **2014**, *507*, 181–189. [CrossRef]
11. Raj, A.; Suthanthiraraj, P.P.A.; Sen, A.K. Pressure-driven flow through PDMS-based flexible microchannels and their applications in microfluidics. *Microfluid. Nanofluidics.* **2018**, *22*, 128. [CrossRef]
12. Hong, J.W.; Quake, S.R. Integrated nanoliter systems. *Nat. Biotechnol.* **2003**, *21*, 1179–1183. [CrossRef] [PubMed]
13. Melin, J.; Quake, S.R. Microfluidic large-scale integration: The evolution of design rules for biological automation. *Annu. Rev. Biophys. Biomol. Struct.* **2007**, *36*, 213–231. [CrossRef] [PubMed]
14. Thorsen, T.; Maerkl, S.J.; Quake, S.R. Microfluidic large-scale integration. *Science* **2002**, *298*, 580–584. [CrossRef]
15. Srinivasan, B.; Lee, J.S.; Hohnbaum, J.; Tung, S.; Kim, J. Performance evaluation of a pneumatic-based micromixer for bioconjugation reaction. In Proceedings of the 2010 5th IEEE International Conference on Nano/micro Engineered and Molecular Systems, Xiamen, China, 20–23 January 2010; pp. 810–814.
16. Wang, X.; Ma, X.; An, L.; Kong, X.; Xu, Z.; Wang, J. A pneumatic micromixer facilitating fluid mixing at a wide range flow rate for the preparation of quantum dots. *Sci. China Chem.* **2013**, *56*, 799–805. [CrossRef]
17. Liu, X.; Li, S. Control method experimental research of micro chamber air pressure via a novel electromagnetic microvalve. In Proceedings of the 2017 4th International Conference on Information Science and Control Engineering, ICISCE, Changsha, China, 24–23 July 2017; pp. 700–705.
18. Lee, J.N.; Park, C.; Whitesides, G.M. Solvent compatibility of poly(dimethylsiloxane)-based microfluidic devices. *Anal. Chem.* **2003**, *75*, 6544–6554. [CrossRef]
19. Nguyen, P.H.; Zhang, W. Design and computational modeling of fabric soft pneumatic actuators for wearable assistive devices. *Sci. Rep.* **2020**, *10*, 9638. [CrossRef]
20. PDMS Elastomeric Film Materials. Available online: https://zhuanlan.zhihu.com/p/149539550 (accessed on 4 September 2022). In Chinese.
21. Hardy, B.S.; Uechi, K.; Zhen, J.; Kavehpour, H.P. The deformation of flexible PDMS microchannels under a pressure driven flow. *Lab Chip* **2009**, *9*, 935–938. [CrossRef]
22. Cui, H.; Li, Z.; Jin, G. Preparation and performance analysis of a PDMS-membrane microvalve. *Microfabr. Technol.* **2004**, *3*, 70–75.
23. Kartalov, E.P.; Scherer, A.; Quake, S.R.; Taylor, C.R.; Anderson, W.F. Experimentally validated quantitative linear model for the device physics of elastomeric microfluidic valves. *J. Appl. Phys.* **2007**, *101*, 064505. [CrossRef]
24. Lee, S.W.; Kim, D.J.; Ahn, Y.; Chai, Y.G. Simple structured polydimethylsiloxane microvalve actuated by external air pressure. *Proc. Inst. Mech. Eng. Part C J. Mech. Eng. Sci.* **2006**, *220*, 1283–1288. [CrossRef]
25. Yang, Q.; Kobrin, P.; Seabury, C.; Narayanaswamy, S.; Christian, W. Mechanical modeling of fluid-driven polymer lenses. *Appl. Opt.* **2008**, *47*, 3658–3668. [CrossRef] [PubMed]
26. Chung, J.; Issadore, D.; Ullal, A.; Lee, K.; Weissleder, R.; Lee, H. Rare cell isolation and profiling on a hybrid magnetic/size-sorting chip. *Biomicrofluidics* **2013**, *7*, 054107. [CrossRef] [PubMed]
27. Liu, X.; Li, S.; Bao, G. Numerical simulation on the response characteristics of a pneumatic micro actuator for microfluidic chips. *J. Lab. Autom.* **2016**, *21*, 412–422. [CrossRef]
28. Cao, Z.; Chen, F.; Bao, N.; He, H.; Xu, P.; Jana, S.; Jung, S.; Lianb, H.; Lu, C. Droplet sorting based on the number of encapsulated particles using a solenoid valve. *Lab Chip* **2013**, *13*, 171–178. [CrossRef] [PubMed]
29. Yang, G. *Elastic-plastic mechanics*, 2nd ed.; Tsinghua University Press: Beijing, China, 2013. (In Chinese)
30. Li, L.; Li, H.; Kou, G.; Yang, D.; Hu, W.; Peng, J.; Li, S. Dynamic camouflage characteristics of a thermal infrared film inspired by honeycomb structure. *J. Bionic Eng.* **2022**, *19*, 458–470. [CrossRef]
31. Li, S.; Jia, H.; Li, M.; Wang, D.; Qin, Z.; Chen, H. Theory and special test method of superelastic constitutive model. *Elastomer* **2011**, *21*, 58–64.
32. Liu, H. *Mechanics of Materials*, 6th ed.; Higher Education Press: Beijing, China, 2017. (In Chinese)
33. Yu, B. Microfluidic Large Scale Integration and Its Application in Image Based Microflow Cytometry. Master's Thesis, University of Waterloo, Waterloo, ON, Canada, 2010; pp. 35–41.
34. Wen, S.; Huang, P. *Theory of Tribology*, 2nd ed.; Tsinghua University Press: Beijing, China, 2008. (In Chinese)
35. Vlassak, J.J.; Nix, W.D. A new bulge test technique for the determination of Young's modulus and Poisson's ratio of thin films. *J. Mater. Res.* **1992**, *7*, 3242–3249. [CrossRef]
36. Yu, J.; Wei, Y. *Finite Element Stress Analysis of Incompressible Hyperelastic Materials*; Southwest Jiaotong University Press: Chengdu, China, 1998; Volume 33, pp. 41–45. (In Chinese)
37. Ying, C. *Gas Transport Theory and Applications*; Tsinghua University Press: Beijing, China, 1990; pp. 50–52.
38. Wu, P.; Little, W.A. Measurement of friction factors for the flow of gases in very fine channels used for microminiature Joule-Thomson refrigerators. *Cryogenics* **1983**, *23*, 273–277.
39. Li, H.; Xu, G.; Li, S. Flow characteristics analysis of Laval type fuel flow control valve. *J. Mech. Electr. Eng.* **2012**, *29*, 1036–1045.

40. Liu, X.; Li, S. Fabrication of a three-Layer PDMS pneumatic microfluidic chip for micro liquid sample operation. *SLAS Technol. Transl. Life Sci. Innov.* **2019**, *25*, 151–161. [CrossRef] [PubMed]
41. Rodríguez, G.A.A.; Rossi, C.; Zhang, K. Multi-physics system modeling of a pneumatic micro actuator. *Sens. Actuators A* **2008**, *141*, 489–498. [CrossRef]
42. GOuyang, G.; Tong, Z.; Gao, W.; Wang, K.; Akram, M.N.; Kartashov, V.; Chen, X.Y. Polymer-based multiple diffraction modulator for speckle reduction. *Proc. SPIE* **2010**, *7387*, 73871F.
43. Lu, X. Research on a Soft Robotic Tongue with Pnuematic Actuation. Master's Thesis, Nanjing University of Science and Technology, Nanjing, China, 2019; pp. 5–6.
44. Qian, P.; Pu, C.; Liu, L.; Lv, P.; Paez, L.M.R. A novel pneumatic actuator based on high-frequency longitudinal vibration friction reduction. *Sens. Actuators A Phys.* **2022**, *344*, 113731. [CrossRef]
45. Lee, Y.-K.; Tabeling, P.; Shih, C.; Ho, C.-M. Characterization of a MEMS-fabricated mixing device. In Proceedings of the ASME 2000 International Mechanical Engineering Congress and Exposition. Micro-Electro-Mechanical Systems (MEMS), Orlando, FL, USA, 5–10 November 2000; pp. 505–511.
46. Maliani, A.D.E.; Hassouni, M.E.; Berthoumieu, Y.; Aboutajdine, D. Generic multivariate model for color texture classification in RGB color space. *Int. J. Multimed. Inf. Retr.* **2014**, *4*, 217–231. [CrossRef]
47. Nazari, M.; Rashidib, S.; Esfahania, J.A. Mixing process and mass transfer in a novel design of induced-charge electrokinetic micromixer with a conductive mixing-chamber. *Int. Commun. Heat Mass Transf.* **2019**, *108*, 104293. [CrossRef]
48. Lee, C.; Fu, L. Recent advances and applications of micromixers. *Sens. Actuators B Chem.* **2018**, *259*, 677–702. [CrossRef]